Author Manuscript

Author Manuscript

Author Manuscript

Author Manuscript

HHS Public Access

Author manuscript

Neuron. Author manuscript; available in PMC 2020 April 03.

Published in final edited form as:

Neuron. 2019 April 03; 102(1): 249–259.e4. doi:10.1016/j.neuron.2019.01.026.

Cortical areas interact through a communication subspace

João D. Semedo[1,2,3,*], **Amin Zandvakili**[5], **Christian K. Machens**[2,†], **Byron M. Yu**[1,4,†], and **Adam Kohn**[5,6,7,†]

[1]Department of Electrical and Computer Engineering, Carnegie Mellon University, Pittsburgh, PA, USA

[2]Champalimaud Research, Champalimaud Centre for the Unknown, Lisbon, Portugal

[3]Department of Electrical and Computer Engineering, Instituto Superior Técnico, Lisbon, Portugal

[4]Department of Biomedical Engineering, Carnegie Mellon University, Pittsburgh, PA, USA

[5]Dominick Purpura Department of Neuroscience, Albert Einstein College of Medicine, Bronx, NY, USA

[6]Department of Ophthalmology and Visual Sciences, Albert Einstein College of Medicine, Bronx, NY, USA

[7]Department of Systems and Computational Biology, Albert Einstein College of Medicine, Bronx, NY, USA

Summary

Most brain functions involve interactions among multiple, distinct areas or nuclei. For instance, visual processing in primates requires the appropriate relaying of signals across many distinct cortical areas. Yet our understanding of how populations of neurons in interconnected brain areas communicate is in its infancy. Here we investigate how trial-to-trial fluctuations of population responses in primary visual cortex (V1) are related to simultaneously-recorded population responses in area V2. Using dimensionality reduction methods, we find that V1-V2 interactions occur through a communication subspace: V2 fluctuations are related to a small subset of V1 population activity patterns, distinct from the largest fluctuations shared among neurons within V1. In contrast, interactions between subpopulations within V1 are less selective. We propose that the communication subspace may be a general, population-level mechanism by which activity can be selectively routed across brain areas.

[*]**Correspondence:** João D. Semedo, Carnegie Mellon University, Department of Electrical and Computer Engineering, Pittsburgh, PA 15213, USA, jsemedo@cmu.edu.

Author Contributions

J.D.S., C.K.M., B.M.Y. and A.K. designed the analyses. J.D.S. performed all the analyses. A.Z. and A.K. designed and performed the experiments. J.D.S., C.K.M., B.M.Y. and A.K wrote the manuscript. C.K.M., B.M.Y. and A.K. contributed equally to this work.

[†]These authors contributed equally to this work.

Declaration of Interests

The authors declare no competing interests.

Publisher's Disclaimer: This is a PDF file of an unedited manuscript that has been accepted for publication. As a service to our customers we are providing this early version of the manuscript. The manuscript will undergo copyediting, typesetting, and review of the resulting proof before it is published in its final citable form. Please note that during the production process errors may be discovered which could affect the content, and all legal disclaimers that apply to the journal pertain.

Author Manuscript Author Manuscript Author Manuscript Author Manuscript

eTOC Blurb

Most brain functions require the selective and flexible routing of neuronal activity between cortical areas. Using paired population recordings from multiple visual cortical areas, Semedo et al. find a population-level mechanism that can achieve this routing, termed a communication subspace.

Introduction

Interactions among brain areas are widely assumed to be essential to most brain functions, yet we are only beginning to understand how neurons in distinct brain areas mediate these interactions. Previous studies of inter-areal interactions have related the spiking activity of pairs of neurons in different areas (Nowak et al., 1999; Roe and Ts'o, 1999; Jia et al., 2013; Pooresmaeili et al., 2014; Oemisch et al., 2015; Ruff and Cohen, 2016), the spiking activity of a neuronal population in one area and a single neuron in another (Truccolo et al., 2010; Zandvakili and Kohn, 2015), the spiking activity of a neuron or group of neurons in one area and the local field potential (LFP) in another (Gregoriou et al., 2009; Salazar et al., 2012; Menzer et al., 2014; Arce-McShane et al., 2016; Wong et al., 2016), the LFPs recorded in different areas (Gregoriou et al., 2009; Salazar et al., 2012; Bosman et al., 2012; Jia et al., 2013; Roberts et al., 2013), or the trial-averaged population activity in distinct areas (Kaufman et al., 2014). These approaches have provided insight into how interaction strength changes with stimulus drive (Nowak et al., 1999; Jia et al., 2013; Roberts et al., 2013), attentional state (Gregoriou et al., 2009; Bosman et al., 2012; Oemisch et al., 2015; Ruff and Cohen, 2016), or task demands (Salazar et al., 2012; Kaufman et al., 2014; Menzer et al., 2014; Pooresmaeili et al., 2014; Arce-McShane et al., 2016; Wong et al., 2016).

These previous approaches fall short, however, of elucidating how the spiking activity of neuronal populations – the signals thought to encode information in the brain – is related across areas on a trial-by-trial basis (Semedo et al., 2014). Pairwise correlations, by definition, ignore structure not evident in the interactions between two individual neurons. LFPs lump the activity of spiking populations into a single summary signal and thereby risk losing much of the richness of area-to-area interactions (Jia et al., 2011; Ray and Maunsell, 2011). Trial-averaging allows one to study how mean signals (e.g., receptive field structure) are related, but not to understand how the moment-by moment changes in activity in one area relate to those in another area (Saalmann et al., 2012; Salazar et al., 2012).

Here we leverage trial-to-trial co-fluctuations of V1 and V2 neuronal population responses, recorded simultaneously in macaque monkeys, to understand the nature of population-level interaction between cortical areas. Within individual brain areas, trial-to-trial fluctuations in activity have yielded important insight into the effects of attention (Cohen and Maunsell, 2009; Mitchell et al., 2009), learning (Gu et al., 2011; Jeanne et al., 2013), stimulus drive (Smith and Kohn, 2008; Churchland et al., 2010), and more. These fluctutations involve multiple dimensions of activity shared among neurons (Yu et al., 2009; Harvey et al., 2012; Ecker et al., 2014; Sadtler et al., 2014; Kaufman et al., 2015; Lin et al., 2015; Rabinowitz et al., 2015; Mazzucato et al., 2016; Williamson et al., 2016), as identified using dimensionality reduction (Cunningham and Yu, 2014). Each of these dimensions represents

Author Manuscript Author Manuscript Author Manuscript Author Manuscript

a characteristic way in which the activities of the recorded neurons covary (referred to as a population activity pattern). It is currently unknown whether all or only a subset of these dimensions are related across brain areas, and which dimensions are involved.

In anesthetized macaque monkeys, we find that interactions between V1 and V2 are similar in strength to those between subpopulations within V1, but that the structure of those interactions is strikingly distinct. V2 activity is related to a small subset of V1 population activity patterns, which are distinct from the largest shared fluctuations among V1 neurons. The selective routing of specific population activity patterns between V1 and V2 can be described by a low-dimensional communication subspace, which defines which activity patterns are effectively relayed between areas. We found that the same low-dimensional structure was present in paired V1-V4 recordings in awake animals, suggesting a general principle of inter-areal interactions. We propose that the communication subspace can be a population-level mechanism by which activity is selectively and flexibly routed between distinct neuronal populations.

Results

We simultaneously recorded the activity of neuronal populations in the output layers (2/3-4B) of V1 (88 to 159 neurons; mean: 112.8) and their primary downstream target, the middle layers of V2 (24 to 37 neurons; mean: 29.4) (Felleman and Essen, 1991) in three sufentanil-anesthetized monkeys (Figure 1A). Neurons consisted of both well-isolated single units and small multi-unit clusters. The recorded V1 and V2 populations had retinotopically-aligned receptive fields, maximizing the probability of direct feedforward interactions (Zandvakili and Kohn, 2015).

We measured neuronal activity as spike counts in 100 ms bins during the presentation of drifting sinusoidal gratings of different orientations. To study how neuronal activity in the two areas is related, we analyzed trial-to-trial response fluctuations to repeated presentations of each grating. These fluctuations involve spiking activity that could propagate between areas, and thus provides a useful window for understanding inter-areal interactions (Fries et al., 2001; Pesaran et al., 2008; Bosman et al., 2012; Saalmann et al., 2012; Salazar et al., 2012). Specifically, we subtracted the appropriate peri-stimulus time histogram from each single-trial response, and then analyzed the residuals for each orientation (henceforth referred to as a data set) separately.

To determine how V1-V2 interactions differ from interactions within V1, we divided the recorded V1 neurons into *source* and *target* populations (Figure 1B). For each data set, we matched the target V1 population to the neuron count and firing rate distribution of the measured V2 population (see STAR Methods). We then related the activity of the same source V1 population separately to the activity of the target V1 population (V1-V1 interaction) and that of the V2 population (V1-V2 interaction).

Strength of population interactions

We first characterized V1-V2 interactions by measuring the degree to which response fluctuations were shared between pairs of neurons (i.e., noise correlations), as in previous

Author Manuscript Author Manuscript Author Manuscript Author Manuscript

inter-areal studies (Nowak et al., 1999; Ruff and Cohen, 2016). The vast majority of V1-V2 pairs had correlations between 0 and 0.2 (Figure 2A, red histogram; average correlation: 0.07 ± 0.06 S.D.). V1-V1 correlations were remarkably similar to those of V1-V2 pairs (Figure 2A, blue histogram; average correlation: 0.07 ± 0.06 S.D.; two-sided Monte Carlo paired permutation test, $p > 0.05$ for difference between V1-V1 and V1-V2). These weak correlations indicate that only a small fraction of a neuron's response variability can be explained by another individual neuron. Indeed, individual source V1 neurons could predict only 1.11 ± 0.03% and 1.35 ± 0.03% of the variability of the target V1 and V2 neurons, respectively (Figure 2B, solid lines).

We next asked how well the variability of the target V1 and V2 neurons could be explained by the source V1 population using multivariate linear regression (see STAR Methods). On average, the source V1 population predicted 15.2 ± 0.7% of the V2 variability (Figure 2B, red histogram), a substantial improvement over the performance afforded by individual V1 neurons. V1-V1 prediction quality was similar to that of the V1-V2 prediction (Figure 2B, blue histogram; 12.9 ± 0.8%; two-sided Monte Carlo paired permutation test, $p < 0.01$ for difference between V1-V1 and V1-V2).

To assess whether the performance of the regression models is reasonable in absolute terms, we implemented a basic model of population interactions using a linear feedforward network. Regression performance for these simulated data was similar to performance on the physiological data either when the target population had Poisson variability or when the observed source population was a subset of the full input population (Figure S1).

In summary, both pairwise analysis and population-based regression models indicate that interactions between areas are similar in strength to those within a cortical area: fluctuations in the source V1 population can be used as effectively for predicting V2 activity as for predicting the fluctuations of other V1 neurons. We next asked whether the structure of these interactions is similar as well.

Structure of population interactions

Consider predicting the activity of a V2 neuron from a population of three V1 neurons using linear regression, as in the preceding section:

$$V2^k = w_1 V1_1{}^k + w_2 V1_2{}^k + w_3 V1_3{}^k$$

where $V2^k$ is the predicted activity of a V2 neuron on the kth trial, $V1_1{}^k$, $V1_2{}^k$ and $V1_3{}^k$ are the corresponding activities of the three V1 neurons on the same trial, and w_1, w_2 and w_3 are the regression weights. We can plot the activity of the V1 population on each trial as a point in a three-dimensional space, where each axis represents the activity of one of the V1 neurons (Figure 3A). The weights can be represented as a *regression dimension*, which captures which aspects of the V1 population activity are predictive of the V2 neuron's activity. Specifically, the location of the V1 activity along the regression dimension is the predicted activity of the V2 neuron (Figure 3A, shading).

Author Manuscript Author Manuscript Author Manuscript Author Manuscript

In a basic multivariate regression model, each V2 neuron has its own regression dimension. These regression dimensions could, in principle, fully span the V1 activity space (Figure 3B). If this were the case, any fluctuation in V1 population activity would be predictive of the fluctuations of one or more V2 neurons (i.e., changing the V1 population activity would change the location of the activity along at least one of the regression dimensions). Alternatively, if the regression dimensions span only a subspace of the V1 activity space (shown as a plane in Figure 3C), certain V1 fluctuations (i.e., those orthogonal to the plane, Figure 3C, dashed line) would not be predictive of V2 fluctuations. We define *predictive dimensions* to be those which reside within the V1 subspace that is predictive of V2 fluctuations, and *private dimensions* as those which do not. The existence of private dimensions within the source population would allow for specific population activity fluctuations to be relayed downstream; any fluctuations along the private dimensions would be hidden from the target population.

To test whether our ability to predict V2 fluctuations involves only a subspace of V1 population activity, we used reduced-rank regression (Izenman, 1975; Kobak et al., 2016), a variant of linear regression in which the regression dimensions are constrained to lie in a low-dimensional subspace (see STAR Methods). If only a few dimensions of V1 activity are predictive of V2, then using a low-dimensional subspace should achieve the same prediction performance as the full regression model. For a representative data set (Figure 4A), only two dimensions were needed to achieve a prediction performance that was indistinguishable from the full regression model (triangle). In contrast, when we applied the same analysis to the target V1 population, six dimensions of the source V1 population activity were needed to reach the performance of the full model (Figure 4B). Across all data sets, consistently fewer dimensions were needed to predict fluctuations in the V2 population (2.2 ± 0.1) compared to the target V1 population (3.5 ± 0.1; one-sided Monte Carlo paired permutation test, $p < 10^{-8}$; Figure 4C).

These results indicate that the V1 fluctuations that are predictive of V2 are confined to a small number of V1 dimensions. Notably, the number of dimensions needed to account for interactions between areas was smaller than the number of dimensions involved in interactions within an area.

The influence of target population dimensionality

A possible explanation for the lower-dimensional interaction between V1-V2 compared to within V1 is that the V2 population activity is itself less complex, or lower dimensional, than the target V1 activity. For example, if the measured V2 population consisted of neurons with identical responses, then predicting those responses would involve the same weighting of V1 activity (i.e., one predictive dimension). More generally, the number of predictive dimensions will depend in part on the dimensionality of the target population activity. All else being equal, the lower the dimensionality of the target population activity, the smaller the number of predictive dimensions will be.

We used factor analysis to test whether the V2 population activity was lower-dimensional than the target V1 population activity. Factor analysis identifies factors (or dimensions) which capture shared activity fluctuations among neurons (Santhanam et al., 2009; Yu et al.,

Author Manuscript Author Manuscript Author Manuscript Author Manuscript

2009; Churchland et al., 2010; Harvey et al., 2012; Ecker et al., 2014; Sadtler et al., 2014; Semedo et al., 2014; Williamson et al., 2016). This analysis revealed that the dimensionality of the V2 activity was higher than that of the target V1 activity (Figure 5A; 5.0 ± 0.2 for V2; 3.7 ± 0.1 for target V1; mean ± S.E.M.; one-sided Monte Carlo paired permutation test, $p < 10^{-8}$). Thus, the smaller number of V2 predictive dimensions cannot be explained by the V2 population response being less complex than the target V1 population response.

To assess how the complexity of the target population influenced the dimensionality of the interactions, we compared the number of predictive dimensions to the dimensionality of the target population activity. For V1-V1 interactions, the number of predictive dimensions closely matched the dimensionality of the target population activity in each data set (Figure 5B, blue points). Although these two estimates of dimensionality are based on different analyses, their similarity suggests that the number of V1 predictive dimensions is as large as possible, given the complexity of the target population response. In contrast, for V1-V2 interactions, the number of predictive dimensions was consistently lower than the dimensionality of the target population (Figure 5B, red points).

The finding that the V1-V2 interaction is lower dimensional than the V2 population activity could arise because the reduced rank-regression model predicted the activity of only a few V2 neurons, ignoring the others. To assess this possibility, we refit the model after removing the three V2 neurons whose activity was best captured by the regression model, a number which corresponded to the largest number of V2 predictive dimensions we observed. Refitting the model after removing these neurons had little effect on the number of estimated predictive dimensions (2.20 ± 0.11 in the original analysis vs. 2.20 ± 0.09 after removing top three V2 neurons; two-sided Monte Carlo paired permutation test, $p > 0.05$), indicating that the small number of predictive dimensions reflects a population-level effect.

We conclude that the difference in the number of V1 and V2 predictive dimensions cannot be explained by the complexity of the respective target population responses, but rather reflects the nature of the interaction between these areas. Whereas the V1-V1 interaction uses as many predictive dimensions as possible, the V1-V2 interaction is more selective and is confined to a small subspace of source V1 population activity, which we term a *communication subspace*.

Notably, this low-dimensional interaction structure was also present in simultaneous population recordings in V1 and V4 of awake monkeys (Figure S2), suggesting that the communication subspace is a general property of population-level interactions between brain areas.

Relationship to source population activity

We next sought to understand the structure of the V1-V2 communication subspace. Specifically, we asked two related questions. First, we examined how the V1 and V2 predictive dimensions are related. Are the predictive dimensions for these target populations aligned or do they capture distinct activity fluctuations within the source V1 population? Second, we examined how the V1-V2 communication subspace relates to the structure of

Author Manuscript Author Manuscript Author Manuscript Author Manuscript

activity within the source V1 population. Is V2 activity predicted by the most dominant fluctuations within V1?

To characterize the relationship between V1 and V2 predictive dimensions, we made use of the fact that these dimensions are both defined within the source V1 activity space and capture the parts of the source population activity that are most relevant for predicting each target population. We thus removed the source V1 activity along the different predictive dimensions (see STAR Methods) and assessed whether the remaining source activity could still be used to predict activity in the target V1 and V2 populations.

We first confirmed that our method for removing activity along predictive dimensions was effective. As expected, our ability to predict V2 fluctuations quickly decreased as we removed the source V1 activity along the dimensions that were most predictive of V2 (Figure 6A, filled circles). Across data sets, average predictive performance vanished when all source activity aligned with the V1-V2 communication subspace had been removed (Figure 6B, filled bars; average normalized performance: -0.005 ± 0.001; value is negative due to cross-validation).

In contrast, after removing the source V1 activity that fell along the top V1 predictive dimensions, we were still able to predict V2 fluctuations (Figure 6A, open circles). Across data sets, we retained a substantial fraction of our ability to predict fluctuations in V2 after removing the same number of V1 predictive dimensions as the number of predictive dimensions in the V1-V2 communication subspace (Figure 6B, open bars; average normalized performance: 0.24 ± 0.01; one-sided Monte Carlo paired permutation test, $p < 10^{-8}$). This indicates that the V2 predictive dimensions are not well aligned with the leading V1 predictive dimensions.

We obtained similar results when predicting fluctuations in the target V1 population (Figure 6C). Across data sets, predictive performance was significantly higher after removing source activity along V2 predictive dimensions (Figure 6D, open bars; 0.31 ± 0.01) than after removing activity along the same number of V1 predictive dimensions (Figure 6D, filled bars; 0.06 ± 0.01; one-sided Monte Carlo paired permutation test, $p < 10^{-8}$). Even after removing all source activity that fell within the V1-V2 communication subspace, we could still predict fluctuations in the target V1 population. Together, these analyses indicate the V1-V2 and V1-V1 interactions not only differ in the number of predictive dimensions, but also involve different patterns of source population activity.

To understand how the V1-V2 communication subspace is related to the structure of the source V1 population activity, we used factor analysis to identify the dimensions of largest shared fluctuations within the source V1 population (termed *dominant dimensions*). We then predicted the activity of V2 neurons using linear regression based on the dominant dimensions only. This analysis is conceptually related to reduced-rank regression, which was used to identify the predictive dimensions. However, rather than identifying the subspace that is best for predicting fluctuations in the target population (as in reduced-rank regression), this analysis identifies a subspace that captures the largest shared fluctuations within the source population and then performs regression in that space.

Author Manuscript Author Manuscript Author Manuscript Author Manuscript

If the dominant source V1 dimensions are able to predict V2 activity as well as the V2 predictive dimensions, for the same number of dimensions, this would indicate that the V1-V2 communication subspace preferentially involves the largest activity fluctuations of the V1 population. However, as shown for a representative data set, the dominant V1 dimensions (Figure 7A, open circles) were not able to predict V2 as well as the predictive dimensions (Figure 7A, filled circles). In contrast, within V1, the predictive and dominant dimensions performed similarly (Figure 7B). Across data sets, predicting V2 fluctuations almost always required more dominant V1 dimensions than V2 predictive dimensions (Figure 7C, red). However, for target V1 fluctuations, dominant dimensions of the source V1 population were nearly as informative as the predictive dimensions (Figure 7C, blue; one-sided Monte Carlo permutation test for difference in the minimum number of dominant dimensions when predicting target V1 and V2, $p < 10^{-8}$ for 1 predictive dimension; $p < 10^{-8}$ for 2 predictive dimensions; $p < 0.01$ for 3 predictive dimensions).

These results indicate that the V1 predictive dimensions are aligned with the largest source V1 fluctuations. The V2 predictive dimensions, however, are distinct: not only are they less numerous, they are not well aligned with the V1 predictive dimensions nor with the largest source V1 fluctuations.

Discussion

Nearly all previous studies of interactions between brain areas have used pairwise spike-spike or spike-LFP analyses. Here we investigated the structure of interactions between areas at the level of neuronal population spiking responses. We found a striking difference in the nature of V1-V1 and V1-V2 interactions, summarized in Figure 7D. V2 activity was related to a small subset of population activity patterns in the source V1 population, and these patterns were distinct from the most dominant shared V1 fluctuations. In contrast, more activity patterns in the source V1 population were relevant for predicting the activity of other V1 neurons, and the dominant fluctuations in the source population were the most predictive. Interactions between areas are thus defined by a communication subspace: V1 activity that lies within the communication subspace is communicated with V2, whereas V1 activity that lies outside this subspace is not.

Our analyses were designed to ensure a fair comparison of V1-V1 and V1-V2 interactions. First, we used the same V1 population to predict target V1 and V2 responses, ruling out any potential differences in the source population. Second, we matched the sizes of the target V1 and V2 populations as well as their firing rate distributions, ruling out differences in these basic target population properties. Third, we were able to predict fluctuations in the target V1 and V2 populations equally well (Figure 2), so our results cannot be attributed to differences in the strength of V1-V1 and V1-V2 interactions. Finally, the spatial receptive fields of both the target V1 and V2 population overlapped those of the source population, and subtle variations in alignment could not explain the differences between V1-V1 and V1-V2 interactions (Figure S3).

It is important to note that the estimated number of predictive and dominant dimensions likely depends on the number of recorded neurons and trials (Williamson et al., 2016).

Author Manuscript Author Manuscript Author Manuscript Author Manuscript

Accordingly, our results do not define the dimensionality of V1-V2 interactions in absolute terms; rather, they indicate that those interactions are low-dimensional relative to V1-V1 interactions. We found that if we analyzed only a portion of the recorded populations or trials, the difference between V1-V1 and V1-V2 interactions was less prominent (Figure S2D-F). Thus, with larger data sets, the difference between these interactions is likely even larger than that we identified.

Dimensionality reduction analyses have provided important insights into neuronal population activity structure and its function (see Cunningham and Yu (2014) for a review). However, such analyses have been applied almost uniquely to population responses recorded in a single brain area, rather than to the study of interactions between areas, as we have done. Two important recent studies have investigated the relationship between activity in motor cortex and muscles (Kaufman et al., 2014; Elsayed et al., 2016). They found that preparatory motor activity avoids the potent (i.e., predictive) dimensions which relate cortical activity to muscles during movement, akin to our finding of private dimensions for V1-V2 interactions. Our work builds upon the strength of those studies by relating trial-to-trial fluctuations in directly connected neuronal populations (i.e., those with functional alignment and in specific cortical laminae; Zandvakili and Kohn (2015)). In addition, we studied the difference in interactions within and between areas, as well as the relationship between predictive and dominant dimensions in the source population.

V2 likely performs non-linear operations on inputs received from V1 (Freeman et al., 2013; Yu et al., 2015). Our approach to understanding V1-V2 interactions was to study local fluctuations around different set points (i.e., the trial-to-trial variability around the mean responses to a particular grating) – which function effectively as local linear perturbations in the non-linear transformation between V1 and V2. Our use of trial-to-trial fluctuations is consistent with most previous studies of inter-areal interactions (Fries et al., 2001; Pesaran et al., 2008; Bosman et al., 2012; Saalmann et al., 2012; Salazar et al., 2012), although these have used entirely distinct analyses such as spike-field coherence. To ensure that our estimates of V1-V2 interactions were not distorted by simple downstream non-linearities, we implemented several feedforward network models with standard non-linearities (e.g., squaring). In all cases, we found our analyses recovered interaction dimensionality that closely matched the dimensionality of the linear weights (Figure S4).

Given this reasoning, how can we be sure that the communication subspaces are not an oddity, perhaps defining private and communicated V1 fluctuations differently for each grating stimulus? First, we confirmed that a communication subspace was evident when we analyzed our grating data sets together (Figure S5). Thus, it is not the case that all V1 population fluctuations that are private during the presentation of one grating stimulus are relayed to V2 during the presentation of another. Consistent with the existence of a shared communication subspace, we also found that the communication subspace defined for responses to one grating could effectively predict responses to other gratings (Figure S6). Second, we analyzed V1-V2 interactions during repeated presentations of brief naturalistic movies. These responses also revealed a communication subspace (Figure S7), indicating that the low-dimensional V1-V2 interactions do not arise from the use of grating stimuli. Finally, we analyzed the relationship between the communication subspace and the mapping

Author Manuscript Author Manuscript Author Manuscript Author Manuscript

of stimulus-driven activity from V1 to V2 (i.e., the PSTHs) and found that the communication subspace was able to capture responses that included stimulus information (Figure S8). Thus, the communication subspace identified using trial-to-trial fluctuations captures important aspects of the inter-areal circuity that is used to relay stimulus information. These lines of evidence together indicate that the communication subspace is a fundamental aspect of V1-V2 interactions.

What is the basis of the communication subspace? One possibility might be that our results reflect global population fluctuations, which involve all neurons increasing and decreasing their activity together (Ecker et al., 2014; Schölvinck et al., 2015; Williamson et al., 2016) and may be more prevalent under anesthesia (Ecker et al. (2014); but see Arieli et al. (1996) and Rabinowitz et al. (2015)). However, since global fluctuations are one-dimensional, they cannot by themselves explain the V1-V2 interactions reported here, which typically involved more than a single dimension. In addition, the most predictive dimensions for the V1-V2 interaction were not well aligned with the largest shared fluctuations in V1, nor with the dimensions that were most predictive of the target V1 activity. Notably, we observed a similar communication subspace in simultaneous population recordings in V1 and V4 of awake monkeys (Figure S2), ruling out any confounding influence of anesthesia.

Another possibility might be that the communication subspace between V1 and V2 reflects feedback from higher cortical areas (e.g., feedback from V4 or MT to V2 and V1). In highly interconnected networks, such as the visual cortex, it is difficult to infer with certainty the source of inputs, especially with correlational methods such as those employed here. However, two pieces of evidence suggest that feedback cannot explain our findings: (1) Feedback connections have coarse retinotopic specificity, with individual axons spanning a relatively large portion of the visual field (Angelucci et al., 2002; Stettler et al., 2002). Our effects, however, are retinotopically specific. That is, when we analyzed additional recording sessions where the V1 and V2 populations had receptive fields that were misaligned by several degrees we found a much weaker V1-V2 interaction that was often well captured by a single predictive dimension (Figure S3). Furthermore this dimension was well aligned with the largest shared fluctuations of the source V1 population. The mismatch between the retinotopic specificity of our results and that of feedback connections suggests that the communication subspace does not arise primarily from feedback; (2) Our V2 recordings were performed in the middle layers, which do not receive feedback and are driven almost exclusively by the superficial layers of V1 (Felleman and Essen, 1991). Consistent with this, we found in these data an elevated probability of V2 spiking several milliseconds after the occurrence of a spike in V1 (Zandvakili and Kohn, 2015). This functional signature also suggests a strong feedforward component to the V1-V2 interaction, though it does not exclude the possibility that feedback signals contribute as well.

An alternative possibility might be that the low-dimensional communication subspace arises because only a small subset of V1 neurons project to V2. There is good evidence for selective connections between between V1 and V2 (Sincich et al., 2010), and V1 and other areas (Glickfeld et al. (2013), but see Han et al. (2018) for a contrary view). However, additional simulations confirmed that our observations do not arise trivially from sparse anatomical projection between source and target areas (Figure S9). Further, we emphasize

Author Manuscript Author Manuscript Author Manuscript Author Manuscript

that while anatomy constrains how activity can be routed in cortex, the flexibility of cognition and perception requires additional mechanisms that allow inter-areal signaling to be adjusted from moment-to-moment, based on task demands (e.g., Saalmann et al. (2012); Salazar et al. (2012)).

We propose instead that the communication subspace is an advantageous design principle of inter-area communication. The ability of a source area to communicate only certain activity patterns while keeping others “private” could be a means for the selective routing of signals between areas. To understand the computational benefit of structuring inter-areal communication in this way, we implemented a simulation which captures the common scenario of a source area projecting to two downstream areas, areas A and B (Figure 8). If each downstream area reads from the source area using a different communication subspace, there will be dimensions of the source population activity that are relayed to area A, but not to area B (Figure 8A), and vice versa (Figure 8B). Crucially, if the interaction between these areas does not involve communication subspaces, then all fluctuations in the source population will be relayed to both downstream areas (Figure 8C). The communication subspace is consequently a population-level mechanism whereby activity can be selectively routed between brain areas.

The selective routing allowed by the communication subspace could be adjusted dynamically, allowing moment-to-moment modulation of interactions between cortical areas. Dynamic routing could be accomplished by altering the structure of population activity in a source area; it need not involve changing the communication subspace itself. Much recent work has shown that the structure of population activity is highly and rapidly malleable, by stimulus drive (Kohn and Smith, 2005; Churchland et al., 2010; Mazzucato et al., 2016), task demands (Cohen and Newsome, 2008; Elsayed et al., 2016; Bondy et al., 2018), attention (Cohen and Maunsell, 2009; Mitchell et al., 2009), learning (Gu et al., 2011; Jeanne et al., 2013), and other factors (Kohn et al., 2016).

Allowing interactions between areas to be modulated by the alignment of population activity with a relevant communication subspace has several advantages over a well-known alternative: defining interaction strength by the phase-alignment of spikes to ongoing oscillations (Fries, 2015) (termed “communication through coherence”, CTC). First, the communication subspace hypothesis does not require coordinated oscillations between the source and target areas, which can be difficult to achieve in practice (Ray and Maunsell, 2015). Instead, the implementation of a communication subspace requires only that the target area takes a particular type of weighted combination of its inputs, namely a linear readout that is low-dimensional. This can be implemented in a linear feedforward network (Salinas and Abbott, 1994; Jazayeri and Movshon, 2006), if the weights for each downstream neuron are defined as linear combinations of the same set of basis “weights” (or predictive dimensions). Second, different target areas (or subpopulations within the same target area) can have different communication subspaces in the same source area (Figure 8). CTC can also route distinct signals to downstream targets by using different oscillations within the source area, each of which is coherent with a different downstream target. However, the number of oscillations that can be distinguished by phase is limited by the

Author Manuscript Author Manuscript Author Manuscript Author Manuscript

temporal precision of neurons, and it is not clear whether the same source neurons can entrain to different oscillations at the same time (Remme et al., 2010).

Our framework for understanding inter-areal population interactions makes clear predictions of how the communication subspace could contribute to behavior, which can be tested in future work. For instance, if attention involves altered inter-areal communication, this could be achieved by better alignment between population responses in a source area and the communication subspace relaying those responses to a relevant downstream area. Similarly, learning could involve achieving population activity patterns that are better aligned with an existing communication subspace (Sadtler et al., 2014), or perhaps altering the communication subspace itself. Finally, the degree to which the effects of perturbation experiments (e.g., patterned optogenetic stimulation) would propagate across areas would depend on their alignment with the relevant communication subspaces. A critical implication of our work is thus that studying how experimental manipulations alter population responses in a given cortical area can be misleading. One must also understand how these altered population responses align with the mapping to downstream areas.

STAR★METHODS

CONTACT FOR REAGENT AND RESOURCE SHARING

Further information and requests for resources and reagents should be directed to and will be fulfilled by João D. Semedo (jsemedo@cmu.edu).

EXPERIMENTAL MODEL AND SUBJECT DETAILS

Animal procedures and recording details have been described in previous work (Smith and Kohn, 2008; Zandvakili and Kohn, 2015). Briefly, animals (macaca fascicularis, male, 2-3 years old) were anesthetized with ketamine (10 mg/kg) and maintained on isoflurane (1-2%) during surgery. Recordings were performed under sufentanil (typically 6-18 microgram/kg/hr) anesthesia. Vecuronium bromide (150 microgram/kg/hr) was used to prevent eye movements. All procedures were approved by the IACUC of the Albert Einstein College of Medicine.

METHOD DETAILS

Visual stimulation and recordings—The data analyzed here represent a subset of those reported in Zandvakili and Kohn (2015), namely those that involved the largest and best retinotopically-aligned populations. V1 activity was recorded using a 96 channel Utah array (400 micron inter-electrode spacing, 1 mm length, inserted to a nominal depth of 600 microns; Blackrock, UT). We recorded V2 activity using a set of electrodes/tetrodes (interelectrode spacing 300 microns) whose depth could be controlled independently (Thomas Recording, Germany). These electrodes were lowered through V1, the underlying white matter, and then into V2. Within V2, we targeted neurons in the input layers. We verified the recordings were performed in the input layers using measurements of the depth in V2 cortex, histological confirmation (in a subset of recordings), and correlation measurements. For complete details see Smith et al. (2013) and Zandvakili and Kohn (2015). Voltage snippets that exceeded a user-defined threshold were digitized and sorted offline.

Author Manuscript Author Manuscript Author Manuscript Author Manuscript

The sampled neurons had spatial receptive fields within 2 – 4° of the fovea, in the lower visual field. Average receptive field size (defined as ± 2 S.D.s of a Gaussian function fit to the data) was 1.22 ± 0.01 deg for V1 and 2.33 ± 0.09 deg for V2.

We measured responses evoked by drifting sinusoidal gratings (1 cyc/°; drift rate of 3 – 6.25 Hz; 2.6 – 4.9° in diameter; full contrast, defined as Michelson contrast (Lmax−Lmin/Lmax +Lmin) where Lmin is 0 cd/m^2 and Lmax is 80 cd/m^2) at 8 different orientations (22.5° steps), on a calibrated CRT monitor placed 110 cm from the animal (1024 × 768 pixel resolution at 100 Hz refresh). Each stimulus was presented 300-400 times for 1.28 seconds. Each presentation was preceded by an interstimulus interval of 1.5 seconds. The duration of each experiment varied from 5 to 7 days.

We recorded neuronal activity in three animals. In two of the animals, we recorded in two different but nearby locations in V2, providing distinct middle-layer populations. We refer to each of these five recordings as a session. We treated responses to each of the 8 stimuli in each session separately, yielding a total of 40 data sets.

Data preprocessing—We counted spikes in 100 ms bins, beginning 160 ms after stimulus onset and spanning a total of 1 second (10 bins per trial). To study how neuronal activity in the two areas is related, we reasoned that any fluctuations in the V1 responses, whether due to changes in the visual stimulus or not, could relate to fluctuations in V2. We therefore subtracted the appropriate peri-stimulus time histogram (PSTH) from each single-trial response, and then analyzed the residuals for each orientation (termed data sets) separately. We confirmed that the temporal structure had little effect on our results by shuffling the data across trials while maintaining the temporal identity; doing so reduced the predictive performance for the V2 population to 0. We found qualitatively similar results for a wide range of bin widths (20ms - 1s). Furthermore, we obtained similar results after z-scoring both the source and target population responses, ruling out the possibility that our results were driven by a few high-firing neurons. For all analyses, we excluded neurons that fired less than 0.5 spikes/s on average, across all trials.

We compared our analyses of V1-V2 interactions to the results of applying the same analyses to a held-out V1 population (V1-V1). The target population in the V1-V1 analyses was a held-out subset of the originally recorded population, which was matched in neuron count to the corresponding V2 population. We also matched the firing rate distribution (mean-matched) to the V2 population separately for each stimulus condition (as in Churchland et al. (2010)). To do so, we binned the firing rate distribution of the V1 and V2 populations (for each neuron, the average firing rate was taken across time and trials for each data set), and determined the common firing rate distribution (i.e., for each firing rate interval, we took the minimum neuron count between the two populations). For each firing rate interval, we then randomly picked this minimum number of neurons from the corresponding bin in each population, without replacement. Because we had many more V1 than V2 neurons, the common distribution usually matched the V2 distribution and we selected an equal number of V1 neurons. The size of the matched populations ranged from 15 to 31 units across data sets (mean: 22.3). The V1 neurons that were not selected for the held-out population defined the source V1 population. V2 neurons that were not selected for

Author Manuscript Author Manuscript Author Manuscript Author Manuscript

the V2 mean-matched population were not used in the analysis. We repeated the mean-matching procedure 25 times, using different random, mean-matched subsets of neurons (and consequently producing a different source population). Results for each data set are based on averages across these repeats. The pairwise correlation (r_{sc}) analysis in Figure 2A was based on a single mean-matching procedure which was done jointly for all stimulus conditions. Statistical evaluation for this analysis was performed after converting r_{sc} to Z-scores using the Fisher transformation (Kohn and Smith, 2005):

$$z = \frac{1}{2}\ln\left(\frac{1 + r_{sc}}{1 - r_{sc}}\right)$$

Regression models—We first related trial-to-trial fluctuations in the source V1 population to those in the target populations using a linear model of the form:

$$Y = XB$$

where X is a $n \times p$ matrix containing the residual activity of the source V1 population and Y is a $n \times q$ matrix containing the residual activity of the target (V1 or V2) population (n represents the number of data points, p and q are the number of neurons in the source and target populations, respectively). The coefficient matrix B is of size $p \times q$. Each of the q columns of B linearly combines the activity of the p neurons in X to predict the activity of one neuron in Y. B can be found using the ordinary least squares (OLS) solution which minimizes the squared prediction error:

$$B_{OLS} = (X^T X)^{-1} X^T Y$$

To reduce overfitting, we used ridge regression (referred to as *full regression model* in the main text), a variant of classical linear regression, which gives the solution $B_{Ridge} = (X^T X + \lambda I)^{-1} X^T Y$, where I is a $p \times p$ identity matrix and λ is a constant that determines the strength of regularization. We chose the value of λ using 10-fold cross-validation. Specifically, we selected the largest λ for which mean performance (across folds) was within one S.E.M. of the best performance, separately for each data set (i.e., for each stimulus condition in each recording session). To quantify model performance, we employed 10-fold nested cross-validation (Friedman et al., 2001).

We sought to test whether the target population activity (V1 or V2) could be predicted using a subspace of the source V1 population activity. In other words, we asked if the linear model $Y = XB$ was still accurate when we impose B to be of a given rank, rank(B) = m. This constrained linear regression problem is known as reduced-rank regression (RRR) (Izenman, 1975; Kobak et al., 2016), and can be solved using the singular value decomposition:

$$B_{RRR} = B_{OLS} V V^T$$

Author Manuscript Author Manuscript Author Manuscript Author Manuscript

where B_{OLS} is the ordinary least squares solution and the columns of the $q \times m$ matrix V contain the top m principal components of the optimal linear predictor $\hat{Y}_{OLS} = XB_{OLS}$. To predict target population activity using RRR, we computed:

$$\hat{Y}_{RRR} = XB_{RRR} = XB_{OLS}VV^T = X\bar{B}V^T$$

where $\bar{B} = B_{OLS}V$ is a matrix of size $p \times m$. The columns of $\bar{B}$ define which dimensions of the source population activity are used when generating predictions: they are the predictive dimensions. The sets of weights used to predict each target neuron (the columns of B_{RRR}) are themselves linear combinations of the columns of $\bar{B}$. Note also that the columns of $\bar{B}$ do not form an orthonormal basis. Rather, they are uncorrelated with respect to the source activity, i.e., $\bar{B}^T\Sigma\bar{B} = D$, where Σ is the covariance matrix of the source population activity and D is a diagonal matrix. Thus, the columns of $\bar{B}$ are linearly independent and rank $(\bar{B}) = m$.

To find the optimal dimensionality for the RRR model (the value of m), we used 10-fold cross-validation and found the smallest number of dimensions for which predictive performance was within one S.E.M. of the peak performance.

Factor analysis—To quantify the dimensionality of the activity in the target populations we used Factor Analysis (FA) (Yu et al., 2009; Williamson et al., 2016). FA is defined by:

$$\mathbf{z} \sim \mathcal{N}(0, I)$$
$$\mathbf{y} \mid \mathbf{z} \sim \mathcal{N}(L\mathbf{z} + \mu, \Psi)$$

where $\mathbf{y}$ is a q-dimensional vector containing the observed residuals at a given time point, L is the $q \times m$ loading matrix that defines the relationship between the m-dimensional ($m < q$) latent variable $\mathbf{z}$ and $\mathbf{y}$, μ is a q-dimensional vector and Ψ is a $q \times q$ diagonal matrix. We estimated the dimensionality of the latent variable $\mathbf{z}$ in two steps: (1) we found the number of dimensions m_{peak} that maximized the cross-validated log-likelihood of the observed residuals; (2) we fitted a FA model with m_{peak} dimensions and chose m, using the eigenvalue decomposition, as the smallest dimensionality that captured 95% of the variance in the shared covariance matrix LL^T. This procedure provides more robust estimates of the FA model dimensionality (Williamson et al., 2016).

Removing activity along the predictive dimensions—In order to remove the source population activity along the predictive dimensions, we projected the source activity onto the subspace that is uncorrelated with the predictive dimensions. Formally, we state that two dimensions defined by the vectors $\mathbf{u}$ and $\mathbf{v}$ are uncorrelated with respect to the source activity matrix X if:

$$\mathbf{u}^T\Sigma\mathbf{v} = 0$$

Author Manuscript Author Manuscript Author Manuscript Author Manuscript

where Σ is the covariance matrix of the source activity. Let matrix $\bar{B}$ contain the predictive dimensions. The set of vectors in the uncorrelated subspace is:

$$\{\mathbf{v} : \bar{B}^T \Sigma \mathbf{v} = 0\}$$

In particular, it will be useful to find an orthonormal basis for this subspace:

$$\{Q : \bar{B}^T \Sigma Q = 0,\ Q^T Q = I\}$$

This can be accomplished using the singular value decomposition (SVD). Start by defining $M = \bar{B}^T \Sigma$ and consider its SVD $M = UDV^T$. Choosing Q as the last $p - m$ columns of V (corresponding to the 0 singular values) yields $MQ = 0$, $Q^T Q = I$, which makes Q an orthonormal basis for the uncorrelated subspace. We then projected the source population onto the uncorrelated subspace, $\hat{X} = XQ$, and predicted target activity using ridge regression between $\hat{X}$ and Y.

We also tested the effect of removing all population activity that was predictive of the target population activity under any stimulus condition by analysing responses to all stimulus conditions together (Figure S5).

Comparing dominant and predictive dimensions—To identify the dominant dimensions in the source population, we fit a FA model, and determined the optimal dimensionality (as described above). Using this FA model, we estimated the latent variables $\hat{\mathbf{z}} = \mathbb{E}[\mathbf{z} \mid \mathbf{y}]$ for each $\mathbf{z}$, then performed an orthonormalization procedure to order the elements of $\mathbf{Z}$ by the amount of shared variance explained (Williamson et al., 2016). This allowed us to predict the target population activity using only the most dominant V1 dimension (first element of orthonormalized $\hat{\mathbf{z}}$), the top two most dominant V1 dimensions (first two elements of orthonormalized $\hat{\mathbf{z}}$), etc. We then compared the performance of the dominant and predictive dimensions for predicting activity of the target populations.

Selective communication simulation—In order to show how a communication subspace can subserve selective communication (Figure 8), we simulated responses in a source population (3 neurons), as well as in two downstream populations (3 neurons each). The responses of each downstream neuron were generated as a linear combination of the activity of the neurons in the source population. In Figure 8A-B, where both downstream areas interact with the source area via communication subspaces, the predictive dimensions for all neurons in each area were chosen to lie within a 2-dimensional subspace. Specifically, we generated these dimensions by creating randomly oriented unit vectors in the xy plane and then rotating these vectors 20° around the r_1 axis for the downstream area A neurons and 40° for the downstream area B neurons. Predictive dimensions for both downstream areas were then rotated 20° around the z axis. In Figure 8C, all predictive dimensions were generated by creating randomly oriented unit vectors in the 3-dimensional source activity space. To generate source activity we drew a sample from a Gaussian process with a squared exponential kernel (length scale $\ell^2 = 0.05$). This sample was then embedded into the 3-

Author Manuscript Author Manuscript Author Manuscript Author Manuscript

dimensional source activity space by projecting the activity along a chosen dimension, i.e., if the Gaussian process sample is represented as a $T \times 1$ vector **x** (where T represents the number of time points), and the chosen dimension is represented by the 3×1 vector **v**, then the 3-dimensional source activity is given by $\mathbf{x}\mathbf{v}^T$. When a communication subspace was present, the source activity was chosen to lie along the private dimension of the relevant area. In Figure 8C, any choice of **v** leads to qualitatively similar results, so we chose it to align with the dimension used in Figure 8B. The response for each downstream neuron is given by the projection of the source activity onto the corresponding predictive dimension.

QUANTIFICATION AND STATISTICAL ANALYSIS

Statistical details can be found in the Results and figure legends. All statistical tests reported in the main text treat the data sets as independent (with the exception of Figure 2A, in which data are pooled across all stimuli, resulting in a single pairwise correlation value per pair per session). Repeating the same statistical tests across the five sessions (i.e., averaging the results across the 8 stimuli for each session) also returned significant results ($p < 0.05$) for all tests, with the exception of Figure 2B, where we can no longer reject the null hypothesis that the average predictive performance is the same when predicting target V1 and V2.

DATA AND SOFTWARE AVAILABILITY

The MATLAB analysis code with sample data is available at https://github.com/joao-semedo/communication-subspace. V1-V2 data are available at the CRCNS data sharing web site, at http://dx.doi.org/10.6080/K0B27SHN.

Supplementary Material

Refer to Web version on PubMed Central for supplementary material.

Acknowledgements

We thank A. Aschner and S. Tanabe for graciously providing the V1-V4 awake recordings in Figure S2, A. Jasper for help in analyzing the V1-V4 awake recordings and A. Motiwala and B. Cowley for invaluable discussions. We also thank M. Cohen, S. Kuhlman, and R. Coen-Cagli for providing feedback on the manuscript. This work was supported by the Fundação para a Ciência e a Tecnologia graduate scholarship SFRH/BD/52069/2012 (J.D.S.), John and Claire Bertucci Graduate Fellowship (J.D.S.), NIH U01 NS094288 (C.K.M.), Simons Collaboration on the Global Brain 364994 (B.M.Y., A.K.), 543009 (C.K.M.), 543065 (b.M.Y.), 542999 (A.K.), NIH CRCNS R01 HD071686 (B.M.Y.), NIH CRCNS R01 NS105318 (B.M.Y.), NSF NCS BCS 1533672 and 1734916 (B.M.Y.), Pennsylvania Department of Health Research Formula Grant SAP 4100077048 under the Commonwealth Universal Research Enhancement program (B.M.Y.), NIH EY016774 (A.K.) and Irma T. Hirschl Trust (A.K.).

References

Angelucci A, Levitt JB, Walton EJ, Hupe J-M, Bullier J, and Lund JS (2002). Circuits for local and global signal integration in primary visual cortex. Journal of Neuroscience, 22(19):8633–8646. [PubMed: 12351737]

Arce-McShane FI, Ross CF, Takahashi K, Sessle BJ, and Hatsopoulos NG (2016). Primary motor and sensory cortical areas communicate via spatiotemporally coordinated networks at multiple frequencies. Proceedings of the National Academy of Sciences, 113(18):5083–5088.

Arieli A, Sterkin A, Grinvald A, and Aertsen A (1996). Dynamics of Ongoing Activity: Explanation of the Large Variability in Evoked Cortical Responses. Science, 273(5283):1868–1871. [PubMed: 8791593]

Author Manuscript Author Manuscript Author Manuscript Author Manuscript

Bondy AG, Haefner RM, and Cumming BG (2018). Feedback determines the structure of correlated variability in primary visual cortex. Nature Neuroscience, page 1.

Bosman C, Schoffelen J-M, Brunet N, Oostenveld R, Bastos A, Womelsdorf T, Rubehn B, Stieglitz T, De Weerd P, and Fries P (2012). Attentional Stimulus Selection through Selective Synchronization between Monkey Visual Areas. Neuron, 75(5):875–888. [PubMed: 22958827]

Churchland MM, Yu BM, Cunningham JP, Sugrue LP, Cohen MR, Corrado GS, Newsome WT, Clark AM, Hosseini P, Scott BB, Bradley DC, Smith MA, Kohn A, Movshon JA, Armstrong KM, Moore T, Chang SW, Snyder LH, Lisberger SG, Priebe NJ, Finn IM, Ferster D, Ryu SI, Santhanam G, Sahani M, and Shenoy KV (2010). Stimulus onset quenches neural variability: a widespread cortical phenomenon. Nature Neuroscience, 13(3):369–378. [PubMed: 20173745]

Cohen MR and Maunsell JHR (2009). Attention improves performance primarily by reducing interneuronal correlations. Nature Neuroscience, 12(12):1594–1600. [PubMed: 19915566]

Cohen MR and Newsome WT (2008). Context-Dependent Changes in Functional Circuitry in Visual Area MT. Neuron, 60(1):162–173. [PubMed: 18940596]

Cunningham JP and Yu BM (2014). Dimensionality reduction for large-scale neural recordings. Nature Neuroscience, 17(11):1500–1509. [PubMed: 25151264]

Ecker A, Berens P, Cotton RJ, Subramaniyan M, Denfield G, Cadwell C, Smirnakis S, Bethge M, and Tolias A (2014). State Dependence of Noise Correlations in Macaque Primary Visual Cortex. Neuron, 82(1):235–248. [PubMed: 24698278]

Elsayed GF, Lara AH, Kaufman MT, Churchland MM, and Cunningham JP (2016). Reorganization between preparatory and movement population responses in motor cortex. Nature Communications, 7:13239.

Felleman DJ and Essen DCV (1991). Distributed Hierarchical Processing in the Primate Cerebral Cortex. Cerebral Cortex, 1(1):1–47. [PubMed: 1822724]

Freeman J, Ziemba CM, Heeger DJ, Simoncelli EP, and Movshon JA (2013). A functional and perceptual signature of the second visual area in primates. Nature Neuroscience, 16(7):974–981. [PubMed: 23685719]

Friedman J, Hastie T, and Tibshirani R (2001). The Elements of Statistical Learning, volume 1 Springer series in statistics Springer, Berlin.

Fries P (2015). Rhythms for Cognition: Communication through Coherence. Neuron, 88(1):220–235. [PubMed: 26447583]

Fries P, Reynolds JH, Rorie AE, and Desimone R (2001). Modulation of Oscillatory Neuronal Synchronization by Selective Visual Attention. Science, 291(5508):1560–1563. [PubMed: 11222864]

Glickfeld LL, Andermann ML, Bonin V, and Reid RC (2013). Cortico-cortical projections in mouse visual cortex are functionally target specific. Nature neuroscience, 16(2):219–226. [PubMed: 23292681]

Gregoriou GG, Gotts SJ, Zhou H, and Desimone R (2009). High-Frequency, Long-Range Coupling Between Prefrontal and Visual Cortex During Attention. Science, 324(5931):1207–1210. [PubMed: 19478185]

Gu Y, Liu S, Fetsch C, Yang Y, Fok S, Sunkara A, DeAngelis G, and Angelaki D (2011). Perceptual Learning Reduces Interneuronal Correlations in Macaque Visual Cortex. Neuron, 71(4):750–761. [PubMed: 21867889]

Han Y, Kebschull JM, Campbell RA, Cowan D, Imhof F, Zador AM, and Mrsic-Flogel TD (2018). The logic of single-cell projections from visual cortex. Nature, 556(7699):51–56. [PubMed: 29590093]

Harvey CD, Coen P, and Tank DW (2012). Choice-specific sequences in parietal cortex during a virtual-navigation decision task. Nature, 484(7392):62–68. [PubMed: 22419153]

Izenman AJ (1975). Reduced-rank regression for the multivariate linear model. Journal of Multivariate Analysis, 5(2):248–264.

Jazayeri M and Movshon JA (2006). Optimal representation of sensory information by neural populations. Nature Neuroscience, 9(5):690–696. [PubMed: 16617339]

Jeanne J, Sharpee T, and Gentner T (2013). Associative Learning Enhances Population Coding by Inverting Interneuronal Correlation Patterns. Neuron, 78(2):352–363. [PubMed: 23622067]

Author Manuscript Author Manuscript Author Manuscript Author Manuscript

Jia X, Smith MA, and Kohn A (2011). Stimulus Selectivity and Spatial Coherence of Gamma Components of the Local Field Potential. Journal of Neuroscience, 31(25):9390–9403. [PubMed: 21697389]

Jia X, Tanabe S, and Kohn A (2013). Gamma and the Coordination of Spiking Activity in Early Visual Cortex. Neuron, 77(4):762–774. [PubMed: 23439127]

Kaufman MT, Churchland MM, Ryu SI, and Shenoy KV (2014). Cortical activity in the null space: permitting preparation without movement. Nature Neuroscience, 17(3):440–448. [PubMed: 24487233]

Kaufman MT, Churchland MM, Ryu SI, and Shenoy KV (2015). Vacillation, indecision and hesitation in moment-by-moment decoding of monkey motor cortex. eLife, 4:e04677. [PubMed: 25942352]

Kobak D, Brendel W, Constantinidis C, Feierstein CE, Kepecs A, Mainen ZF, Qi X-L, Romo R, Uchida N, and Machens CK (2016). Demixed principal component analysis of neural population data. eLife, 5:e10989. [PubMed: 27067378]

Kohn A, Coen-Cagli R, Kanitscheider I, and Pouget A (2016). Correlations and Neuronal Population Information. Annual Review of Neuroscience, 39(1):237–256.

Kohn A and Smith MA (2005). Stimulus Dependence of Neuronal Correlation in Primary Visual Cortex of the Macaque. The Journal of Neuroscience, 25(14):3661–3673. [PubMed: 15814797]

Lin I-C, Okun M, Carandini M, and Harris K (2015). The Nature of Shared Cortical Variability. Neuron, 87(3):644–656. [PubMed: 26212710]

Mazzucato L, Fontanini A, and La Camera G (2016). Stimuli Reduce the Dimensionality of Cortical Activity. Frontiers in Systems Neuroscience, 10.

Menzer DL, Rao NG, Bondy A, Truccolo W, and Donoghue JP (2014). Population interactions between parietal and primary motor cortices during reach. Journal of Neurophysiology, 112(11): 2959–2984. [PubMed: 25210154]

Mitchell JF, Sundberg KA, and Reynolds JH (2009). Spatial Attention Decorrelates Intrinsic Activity Fluctuations in Macaque Area V4. Neuron, 63(6):879–888. [PubMed: 19778515]

Nowak LG, Munk MHJ, James AC, Girard P, and Bullier J (1999). Cross-Correlation Study of the Temporal Interactions Between Areas V1 and V2 of the Macaque Monkey. Journal of Neurophysiology, 81(3):1057–1074. [PubMed: 10085333]

Oemisch M, Westendorff S, Everling S, and Womelsdorf T (2015). Interareal Spike-Train Correlations of Anterior Cingulate and Dorsal Prefrontal Cortex during Attention Shifts. Journal of Neuroscience, 35(38):13076–13089. [PubMed: 26400938]

Pesaran B, Nelson MJ, and Andersen RA (2008). Free choice activates a decision circuit between frontal and parietal cortex. Nature, 453(7193):406–409. [PubMed: 18418380]

Pooresmaeili A, Poort J, and Roelfsema PR (2014). Simultaneous selection by object-based attention in visual and frontal cortex. Proceedings of the National Academy of Sciences, 111(17):6467–6472.

Rabinowitz NC, Goris RL, Cohen M, and Simoncelli EP (2015). Attention stabilizes the shared gain of V4 populations. eLife, 4:e08998. [PubMed: 26523390]

Ray S and Maunsell JHR (2011). Different Origins of Gamma Rhythm and High-Gamma Activity in Macaque Visual Cortex. PLOS Biol, 9(4):e1000610. [PubMed: 21532743]

Ray S and Maunsell JHR (2015). Do gamma oscillations play a role in cerebral cortex? Trends in Cognitive Sciences, 19(2):78–85. [PubMed: 25555444]

Remme MWH, Lengyel M, and Gutkin BS (2010). Democracy-Independence Trade-Off in Oscillating Dendrites and Its Implications for Grid Cells. Neuron, 66(3):429–437. [PubMed: 20471355]

Roberts M, Lowet E, Brunet N, Ter Wal M, Tiesinga P, Fries P, and De Weerd P (2013). Robust Gamma Coherence between Macaque V1 and V2 by Dynamic Frequency Matching. Neuron, 78(3):523–536. [PubMed: 23664617]

Roe AW and Ts'o DY (1999). Specificity of Color Connectivity Between Primate V1 and V2. Journal of Neurophysiology, 82(5):2719–2730. [PubMed: 10561440]

Ruff DA and Cohen MR (2016). Attention Increases Spike Count Correlations between Visual Cortical Areas. The Journal of Neuroscience, 36(28):7523–7534. [PubMed: 27413161]

Author Manuscript Author Manuscript Author Manuscript Author Manuscript

Saalmann YB, Pinsk MA, Wang L, Li X, and Kastner S (2012). The Pulvinar Regulates Information Transmission Between Cortical Areas Based on Attention Demands. Science, 337(6095):753–756. [PubMed: 22879517]

Sadtler PT, Quick KM, Golub MD, Chase SM, Ryu SI, Tyler-Kabara EC, Yu BM, and Batista AP (2014). Neural constraints on learning. Nature, 512(7515):423–426. [PubMed: 25164754]

Salazar RF, Dotson NM, Bressler SL, and Gray CM (2012). Content-Specific Fronto-Parietal Synchronization During Visual Working Memory. Science, 338(6110):1097–1100. [PubMed: 23118014]

Salinas E and Abbott LF (1994). Vector reconstruction from firing rates. Journal of Computational Neuroscience, 1(1–2):89–107. [PubMed: 8792227]

Santhanam G, Yu BM, Gilja V, Ryu SI, Afshar A, Sahani M, and Shenoy KV (2009). Factor-Analysis Methods for Higher-Performance Neural Prostheses. Journal of Neurophysiology, 102(2):1315–1330. [PubMed: 19297518]

Schölvinck ML, Saleem AB, Benucci A, Harris KD, and Carandini M (2015). Cortical State Determines Global Variability and Correlations in Visual Cortex. The Journal of Neuroscience, 35(1):170–178. [PubMed: 25568112]

Semedo J, Zandvakili A, Kohn A, Machens CK, and Yu BM (2014). Extracting Latent Structure From Multiple Interacting Neural Populations. In Advances in Neural Information Processing Systems 27, pages 2942–2950.

Sincich LC, Jocson CM, and Horton JC (2010). V1 Interpatch Projections to V2 Thick Stripes and Pale Stripes. Journal of Neuroscience, 30(20):6963–6974. [PubMed: 20484638]

Smith MA, Jia X, Zandvakili A, and Kohn A (2013). Laminar dependence of neuronal correlations in visual cortex. Journal of Neurophysiology, 109(4):940–947. PMID: 23197461. [PubMed: 23197461]

Smith MA and Kohn A (2008). Spatial and Temporal Scales of Neuronal Correlation in Primary Visual Cortex. The Journal of Neuroscience, 28(48):12591–12603. [PubMed: 19036953]

Stettler DD, Das A, Bennett J, and Gilbert CD (2002). Lateral connectivity and contextual interactions in macaque primary visual cortex. Neuron, 36(4):739–750. [PubMed: 12441061]

Truccolo W, Hochberg LR, and Donoghue JP (2010). Collective dynamics in human and monkey sensorimotor cortex: predicting single neuron spikes. Nature Neuroscience, 13(1):105–111. [PubMed: 19966837]

Williamson RC, Cowley BR, Litwin-Kumar A, Doiron B, Kohn A, Smith MA, and Yu BM (2016). Scaling Properties of Dimensionality Reduction for Neural Populations and Network Models. PLOS Computational Biology, 12(12):e1005141. [PubMed: 27926936]

Wong YT, Fabiszak MM, Novikov Y, Daw ND, and Pesaran B (2016). Coherent neuronal ensembles are rapidly recruited when making a look-reach decision. Nature Neuroscience, 19(2):327–334. [PubMed: 26752158]

Yu BM, Cunningham JP, Santhanam G, Ryu SI, Shenoy KV, and Sahani M (2009). Gaussian-Process Factor Analysis for Low-Dimensional Single-Trial Analysis of Neural Population Activity. Journal of Neurophysiology, 102(1):614–635. [PubMed: 19357332]

Yu Y, Schmid AM, and Victor JD (2015). Visual processing of informative multipoint correlations arises primarily in V2. eLife, 4:e06604. [PubMed: 25915622]

Zandvakili A and Kohn A (2015). Coordinated Neuronal Activity Enhances Corticocortical Communication. Neuron, 87(4):827–839. [PubMed: 26291164]

Author Manuscript Author Manuscript Author Manuscript Author Manuscript

Highlights

- Visual cortical areas interact through a communication subspace (CS)
- The CS defines which activity patterns in a source area relate to downstream activity
- The largest activity patterns in a source area are not matched to the CS
- The CS allows for selective and flexible routing of population signals between areas

Author Manuscript Author Manuscript Author Manuscript Author Manuscript

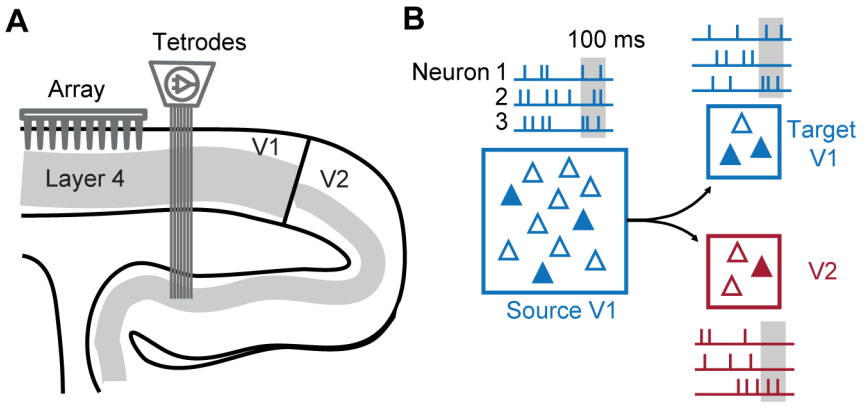

Figure 1. V1 and V2 recordings.

(A) Schematic showing a sagittal section of occipital cortex and the arrangement of the recording apparatus. We simultaneously recorded V1 population activity using a 96-channel Utah array and V2 population activity using a set of movable electrodes and tetrodes.

(B) We related activity of the same V1 source population to a target V1 population and a V2 population. In this illustration, each triangle represents a neuron and the filled triangles indicate active neurons. Spike counts were taken in 100 ms bins.

Author Manuscript Author Manuscript Author Manuscript Author Manuscript

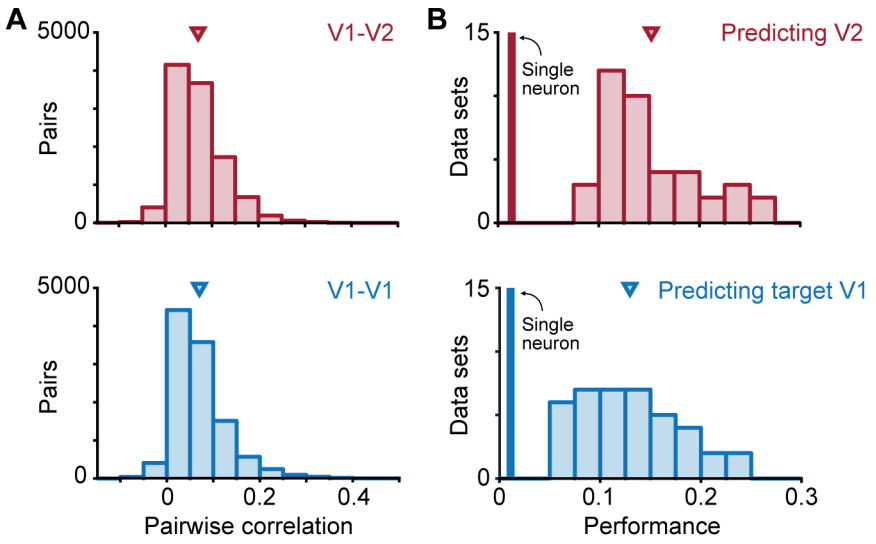

Figure 2. V1-V1 and V1-V2 interactions are similar in strength.

(A) Pairwise correlation histograms for pairs of V1-V2 (red) and V1-V1 (blue) neurons. Triangles indicate average pairwise correlation. Total number of pairs in each histogram n = 10, 944.

(B) Prediction performance for V1-V2 (red) and V1-V1 (blue). Prediction was performed using a single V1 neuron at a time (solid lines) or using the entire source V1 population (histograms; triangles indicate mean). Prediction performance for each data set is defined as the average cross-validated r^2 across all selections of the target and source V1 populations.

Author Manuscript Author Manuscript Author Manuscript Author Manuscript

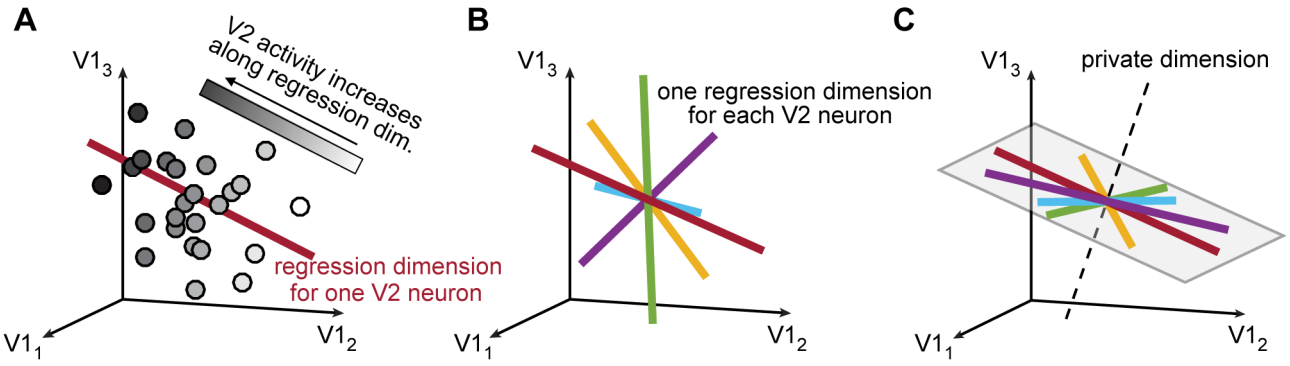

Figure 3. Illustration of a low-dimensional interaction.

(A) Graphical depiction of linear regression between a population of V1 neurons and one V2 neuron. Each circle represents the activity recorded simultaneously in V1 (three neurons) and V2 (one neuron) during one timestep (100 ms). The position of the circle represents the V1 population activity and its shading represents the activity of the V2 neuron. The activity of the V2 neuron increases along the regression dimension (red line).

(B) High-dimensional interaction. The regression dimensions for different V2 neurons (one regression dimension per V2 neuron) span the entire V1 population space.

(C) Low-dimensional interaction. The regression dimensions for different V2 neurons span a subspace of the V1 population space. In this illustration, all regression dimensions lie in a 2-dimensional subspace (the grey plane). The basis vectors for this subspace are called predictive dimensions. Thus, two predictive dimensions are sufficient to capture the between area interaction. All dimensions that are not predictive of V2, and therefore lie outside of this subspace, are called private dimensions.

Author Manuscript Author Manuscript Author Manuscript Author Manuscript

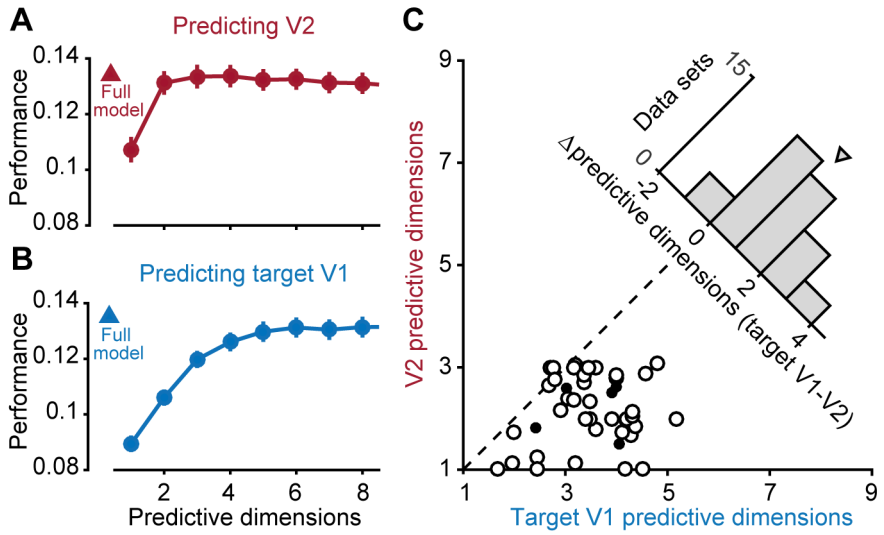

Figure 4. V1-V2 interactions use only a small number of dimensions.

(A) Predicting V2 activity. The number of predictive dimensions (red circles; reduced-rank regression) needed to achieve full predictive performance (red triangle; ridge regression) is small (in this case, 2 dimensions). Across all data sets, reduced-rank regression achieved nearly the same performance as the full regression model (0.150 ± 0.007 for reduced-rank regression versus 0.152 ± 0.007 for the full regression model). The predictive performance slightly decreases with the number of predictive dimensions due to cross-validation. Error bars indicate S.E.M. across cross-validation folds.

(B) Predicting target V1 activity. The number of predictive dimensions (blue circles; reduced-rank regression) needed to achieve full predictive performance (blue triangle; ridge regression) is large (in this case, 6 dimensions). Across all data sets, predictive performance was again similar for reduced-rank regression (0.123 ± 0.008) and the full regression model (0.129 ± 0.008).

(C) The optimal number of predictive dimensions is smaller for predicting V2 than target V1. Each open circle corresponds to one data set. Filled circles indicate averages across data sets for each of the 5 sessions (see STAR Methods). Inset shows the difference between the optimal number of predictive dimensions needed when predicting the target V1 and V2 populations (target V1 minus V2).

Author Manuscript Author Manuscript Author Manuscript Author Manuscript

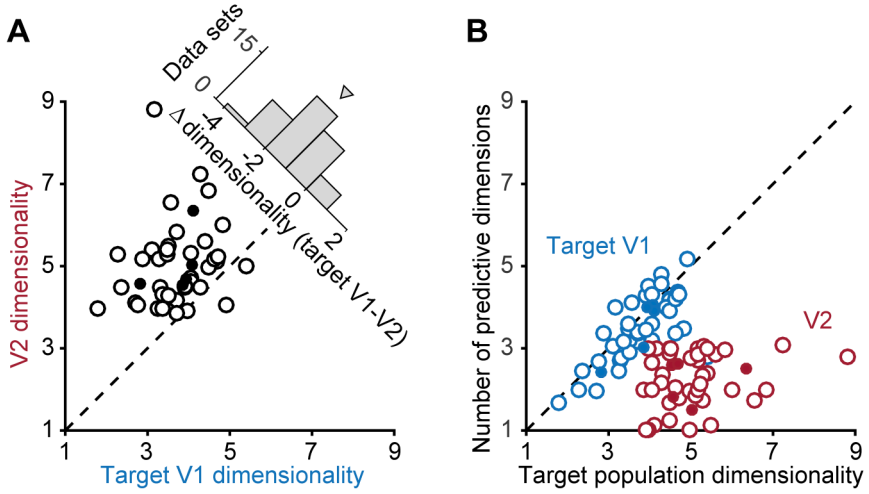

Figure 5. Low-dimensional V1-V2 interaction is not due to low-dimensional V2 activity.

(A) Population activity is more complex in V2 than in target V1. Each open circle corresponds to one data set. Filled circles indicate averages across datasets for each of the 5 sessions. Inset shows the difference between the dimensionality (target V1 minus V2) of the population activity in target V1 and V2.

(B) V1 and V2 interact through a communication subspace. The number of predictive dimensions identified for the V1-V2 interaction was always smaller than the dimensionality of the V2 population activity (red circles). The number of predictive dimensions required when predicting target V1 population activity was similar to the dimensionality of the target V1 population (blue circles). Each open circle corresponds to one data set. Filled circles indicate averages across data sets for each of the 5 sessions.

Author Manuscript Author Manuscript Author Manuscript Author Manuscript

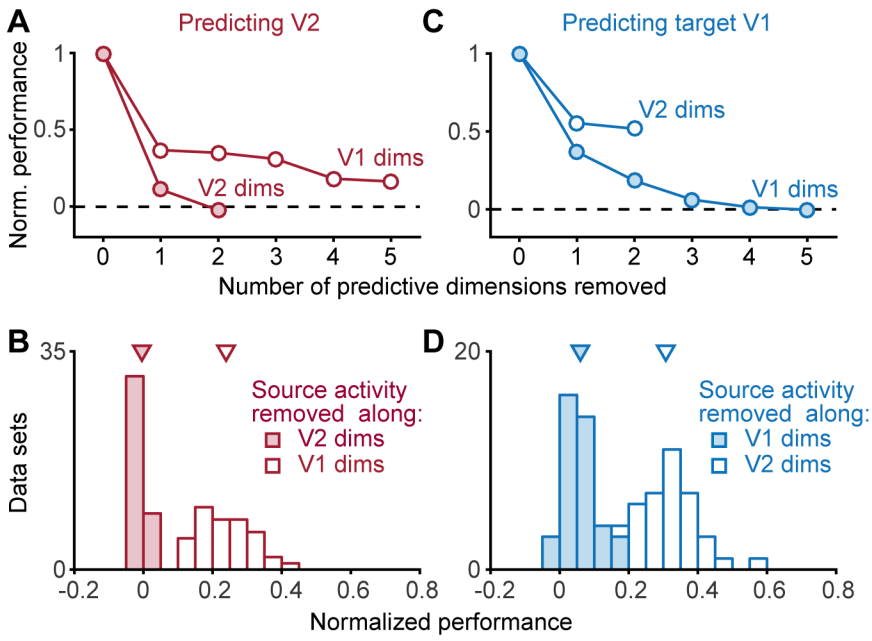

Figure 6. V2 predictive dimensions are not aligned with target V1 predictive dimensions.

(A) Source V1 activity outside of the V1 predictive dimensions is still predictive of V2 activity. V2 predictive performance quickly decreased as we removed the source V1 activity along the V2 predictive dimensions (filled circles). Removing the source V1 activity along the target V1 predictive dimensions had a smaller impact on V2 predictive performance (open circles). Predictive performance was normalized by the performance of the reduced-rank regression model when no activity was removed. S.E.M. is smaller than plotted circles.

(B) Across all data sets, removing all V2 predictive dimensions drove the V2 predictive performance to 0, as expected (red histogram). Removing the same number of V1 predictive dimensions, had a smaller impact on performance (white histogram), as we could still account for roughly one fifth of the predictable activity in V2.

(C) Source V1 activity outside of the V1-V2 communication subspace still accounts for a substantial part of the explained activity in target V1. Target V1 predictive performance decreased faster when removing source V1 activity along the target V1 predictive dimensions (filled circles), when compared to removing source activity along the V2 predictive dimensions (open circles). S.E.M. is smaller than plotted circles.

(D) Across all datasets, even after removing all source activity that was predictive of V2, we could still account for approximately a third of the predictable activity in target V1 (white histogram). Removing the same number of target V1 predictive dimensions had a much larger effect on target V1 predictive performance (blue histogram).

Author Manuscript Author Manuscript Author Manuscript Author Manuscript

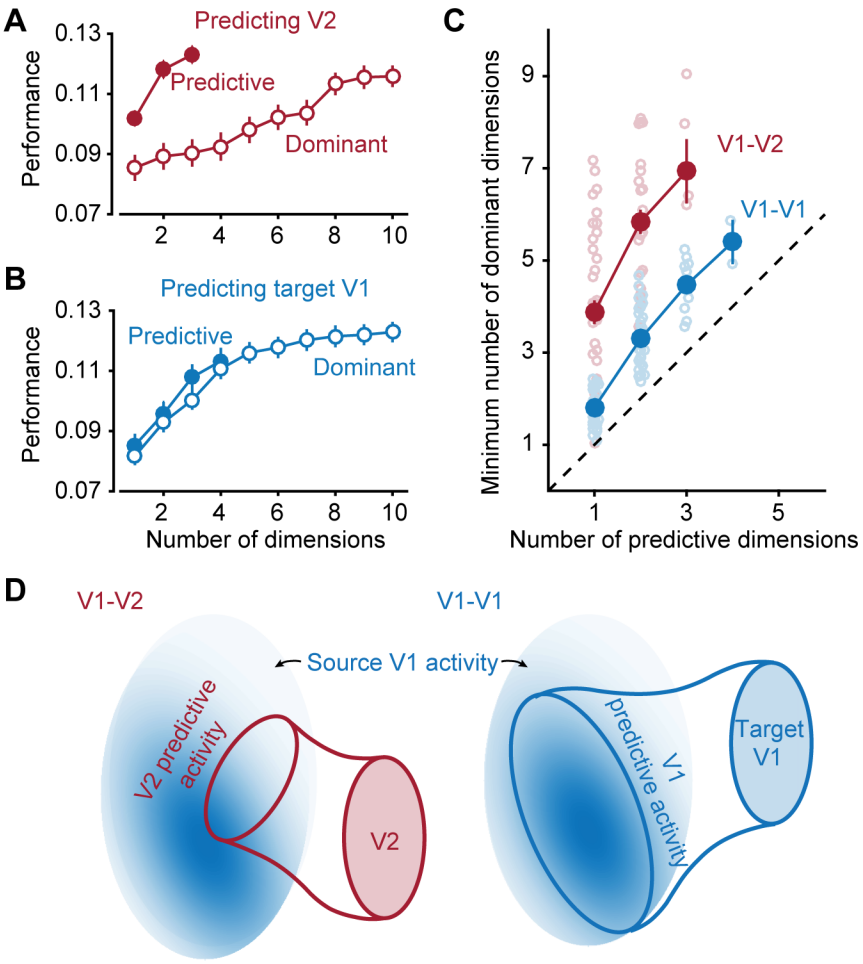

Figure 7. The dominant dimensions of V1 are not the most predictive of V2.

(A) Predicting V2 activity using dominant and predictive dimensions. Dominant dimensions (open circles, factor-analysis regression) carried less predictive power than the same number of predictive dimensions (filled circles, reduced-rank regression). Error bars indicate S.E.M. across cross-validation folds.

(B) Predicting target V1 activity using dominant and predictive dimensions. Predictive performance using dominant dimensions (open circles, factor-analysis regression) was similar to the predictive performance obtained for the same number of predictive dimensions (filled circles, reduced-rank regression). Error bars indicate S.E.M. across cross-validation folds.

(C) For a given number of predictive dimensions, a larger number of dominant dimensions was required to reach (within a S.E.M., across folds) the same V2 predictive performance (red circles). When predicting target V1 activity, the number of dominant dimensions needed was only slightly greater than the number of predictive dimensions (blue circles). Error bars indicate S.E.M. across datasets. Faded circles show results for each data set, and were horizontally jittered for visual clarity.

(D) Left: Schematic of V1-V2 results. Only a small number of activity patterns in the source V1 population was predictive of the V2 population. These predictive activity patterns did not

correspond to the dominant patterns in the source V1 population. Large blue ellipse represents the set of all activity patterns observed in the source V1 population. Darker shading indicates more dominant activity patterns. Right: Schematic of V1-V1 results. A large number of activity patterns in the source V1 population was predictive of the target V1 population. These predictive activity patterns corresponded to the dominant patterns in the source V1 population.

Author Manuscript Author Manuscript Author Manuscript Author Manuscript

Author Manuscript Author Manuscript Author Manuscript Author Manuscript

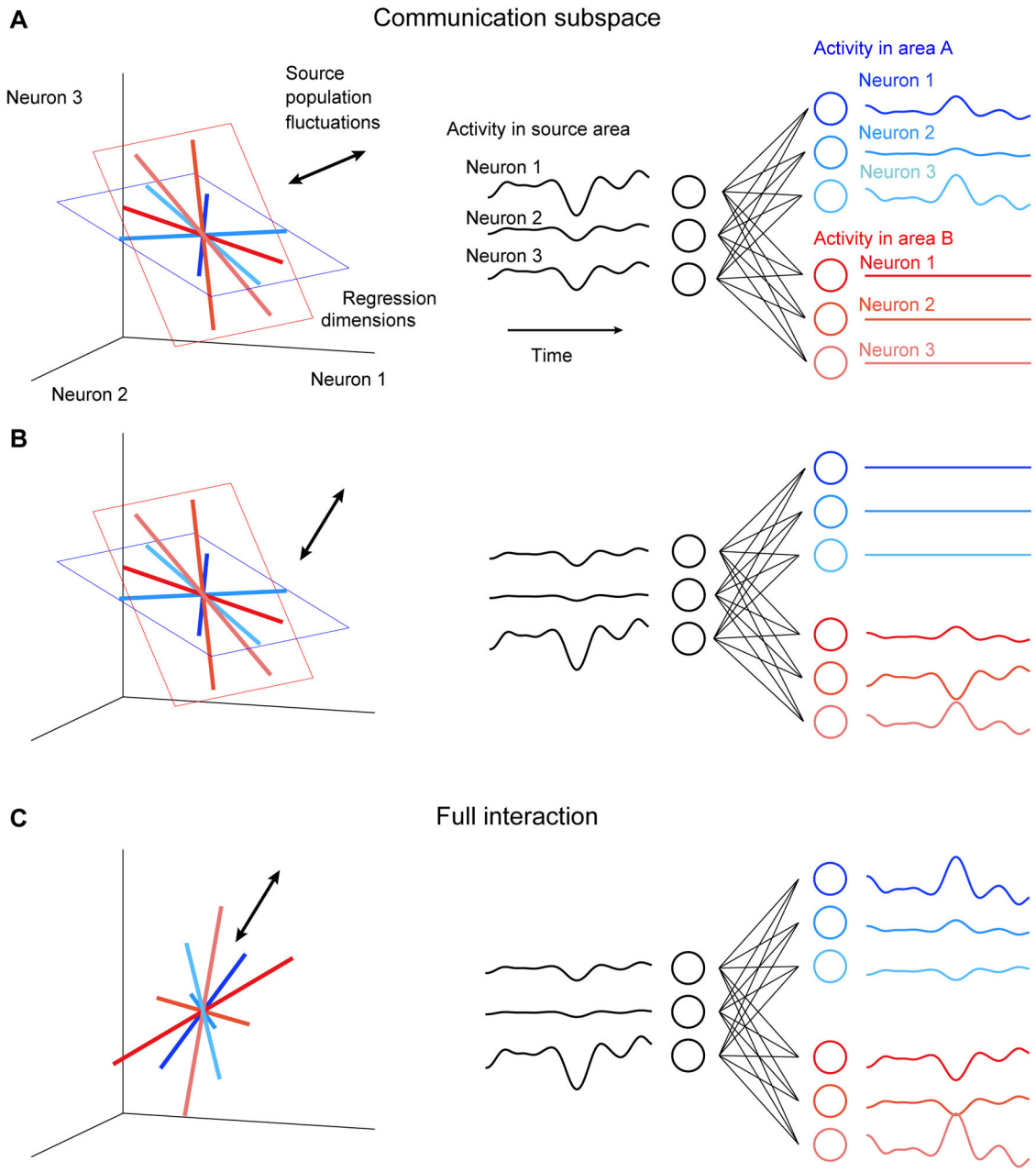

Figure 8. Communication subspaces enable selective communication with multiple downstream areas.

(A) Communication subspace: activity in source area influences downstream area A, but not area B. Left panel: Each of the coordinate axes represents the activity of one source neuron. Each colored line represents the regression dimension of one neuron in area A (blue) or area B (red). Blue plane corresponds to the communication subspace for area A. Red plane corresponds to the communication subspace for area B. Source population fluctuations are indicated by the black arrow. Right panel: The activity of three source neurons (black, corresponding to the source population fluctuations indicated by the black arrow in the left

Author Manuscript Author Manuscript Author Manuscript Author Manuscript

panel) is mapped to the activity of three neurons in area A (blue) and three neurons in area B (red).

(B) Communication subspace: activity in source area influences downstream area B, but not area A. Same conventions as in panel (A). The only difference from panel (A) is the direction of source population fluctuations (i.e., the population activity patterns produced in the source area).

(C) Full interaction: activity in source area influences both downstream areas. Same conventions as in panel (A).